Errandonea, D.; Gomis Hilario, O.; García-Domene, B.; Pellicer Porres, J.; Katari, V.; Achary, SN.; Tyagi, AK.... (2013). New polymorph of InVO4: A high-pressure structure with six-coordinated vanadium. Inorganic Chemistry. 52(21):12790-12798. doi:10.1021/ic402043x.

New polymorph of $InVO_4$: A high-pressure structure with six-coordinated vanadium

Daniel Errandonea,[†] *Oscar Gomis,*[‡] *Braulio García-Domene,*[†] *Julio Pellicer-Porres,*[†] *Vasundhara Katari,*[§] *S. Nagabhusan Achary,*[§] *Avesh K. Tyagi,*[§] *and Catalin Popescu*[⊥]

[†]Departamento de Física Aplicada-ICMUV, Universidad de Valencia, MALTA Consolider Team, Edificio de Investigación, C/Dr. Moliner 50, 46100 Burjassot, Valencia, Spain.

[‡]Centro de Tecnologías Físicas, Universitat Politecnica de Valencia, Camino de Vera s/n, 46022 Valencia, Spain

[§]Chemistry Division, Bhabha Atomic Research Centre, Trombay, Mumbai 400085, India

[⊥]CELLS-ALBA Synchrotron Light Facility, Cerdanyola, 08290 Barcelona, Spain

KEYWORDS: orthovanadates, high pressure, phase transitions, $CrVO_4$-type structure, wolframite, X-ray diffraction, Raman spectroscopy.

ABSTRACT: A new wolframite-type polymorph of $InVO_4$ is identified under compression near 7 GPa by in situ high-pressure (HP) X-ray diffraction (XRD) and Raman spectroscopic investigations on the stable orthorhombic $InVO_4$. The structural transition is accompanied by a large volume collapse ($\Delta V/V$ = -14%) and a drastic increase in bulk modulus (from 69 to 168 GPa). Both techniques also show the existence of a third phase coexisting with the low- and high-pressure phases in a limited pressure range close to the transition pressure. XRD studies revealed a highly anisotropic compression in orthorhombic $InVO_4$. In addition the compressibility becomes non-linear in the HP polymorph. The volume collapse in the lattice is related to an increase of the polyhedral coordination around the vanadium atoms. The transformation is not fully reversible. The drastic change in the polyhedral arrangement observed at the transition is indicative of a reconstructive phase transformation. The HP phase here found is the only modification of $InVO_4$ reported till date with six-fold coordinated vanadium atoms. Finally, Raman frequencies and pressure coefficients in the low- and high-pressure phases of $InVO_4$ are reported.

1. Introduction

$CrVO_4$-type ABO_4 oxides (where A = Cr, Fe, In, Ti, Tl; B = As, P, V) are of interest due to their wide physical properties which lead to several technological uses. Applications include photovoltaic cells for solar energy utilization, catalysts for water splitting, electrolyte for lithium ion batteries, and active material for gas sensors among others [1-7]. The prototype structure of the $CrVO_4$-type structure, represented by orthorhombic $CrVO_4$ [space group (SG) *Cmcm*, Z = 4], consists of chains of nearly regular edge-sharing octahedra of CrO_6 which are linked together by tetrahedral VO_4 groups [1]. The most stable phase of indium orthovanadate ($InVO_4$) belongs to the $CrVO_4$-type family. This vanadate has been investigated in a number of studies due to its potential for applications as catalyst for production of hydrogen by visible-light driven water splitting [2-7]. From optical-absorption spectroscopic studies, an indirect band gap of 3.2 eV and a sub-band-gap absorption near 2.5 eV were reported for $InVO_4$ [3]. Band-gap values smaller than 2 eV have been also reported [4]. Another interesting aspect of $InVO_4$ is that its crystal structure has a significant fraction of free space which facilitates intercalation of cations like lithium [8,9] and the creation of intrinsic-defect structures with cation or anion interstitials [5].

Different preparation and temperature conditions can lead to different polymorphic forms of $InVO_4$, viz. monoclinic $InVO_4$-I (SG *C2/m*), orthorhombic $InVO_4$-III: (SG *Cmcm*) and an undetermined structure $InVO_4$-II [10-13]. In spite of the ambiguities about the structure of $InVO_4$-II, it is believed that the three known polymorphs of $InVO_4$ have InO_6 octahedra and VO_4 tetrahedra as building blocks of the crystal structure. The orthorhombic form ($InVO_4$-III) is the most stable phase in the In_2O_3-V_2O_5 system. Even though $InVO_4$ has several interesting properties, in contrast with other ABO_4 oxides [3,5,14-19], the knowledge of its fundamental crystal chemistry under non-ambient conditions is limited. As the $CrVO_4$-type structure, where the cation coordination numbers (CN) are 6:4, $InVO_4$-III has intermediate structural motifs between silica analogue structures (CN 4:4) and zircon or scheelite-type structures (CN 8:4). Several authors have proposed that $CrVO_4$-structured oxides can undergo phase transitions under pressure to structures having higher coordination numbers of either or both cations [15-19]. High-pressure (HP) studies on silica analogue $AlPO_4$ have shown a sequence of transitions from the berlinite-type to the $CrVO_4$-type structure and then to a distorted $CaCl_2$-type structure with six-fold coordination of both cations [20,21]. On top of that, theoretical calculations have

predicted a $CrVO_4$-type → zircon → scheelite → wolframite HP structural sequence for $CrVO_4$-type $InPO_4$ and $TiPO_4$ [22]. Though a number of HP structural studies have been reported for zircon-, scheelite- or quartz-type ABO_4 compounds, similar research on $CrVO_4$-type materials is scarce [1,15,19,22-24]. In particular, Young and Schwartz had prepared HP phases in $CrVO_4$ and $FeVO_4$ [23,24]. These phases have been obtained combining high pressure and temperature (e.g. 6 GPa and 750ºC) [23]. A rutile-type cation disordered structure has been assigned to them. Thus they are expected to have six-fold coordinated vanadium. However, this hypothesis has not been confirmed by full structural refinements. Rutile-type $CrVO_4$ has also been obtained by the mechanochemical reaction of Cr_2O_3 and V_2O_5 [25]. Then, a possible formation of post $CrVO_4$-type structures with an increased coordination number of vanadium can be expected at relatively low pressure compared to the analogous phosphates where the coordination number of phosphorous remains four up to 70 GPa. According to Zou et al. [7], compounds like $InVO_4$ in case of having six-coordinated vanadium may show maximum efficiency for the splitting of water molecules by visible light. However, no such polymorphs except the aforementioned structures have been reported till date. In this study we have successfully demonstrated the formation of a wolframite-type structure of $InVO_4$ in which both In and V are six coordinated by oxygen. Based upon detail in situ HP X-ray diffraction (XRD) and Raman scattering measurements we concluded that a wolframite-type phase can be prepared at moderate high-pressure conditions ($P \approx 7.2$ GPa) and room temperature. The crystal structure of the new HP phase has been determined. Further, to understand the HP structural behavior and lattice-dynamics properties of the orthorhombic and new phase of $InVO_4$, XRD up to 24 GPa and Raman spectroscopy up to 17 GPa were carried out. The pressure dependence of unit-cell parameters and Raman-mode frequencies are discussed in this manuscript.

2. Experimental methods

Polycrystalline $InVO_4$ was synthesized by solid-state reaction of appropriate amounts of In_2O_3 (99.9 %, Aldrich), and V_2O_5 (99.5 %, Riedel-de Haën). A homogeneous mixture of the reactants was heated at 973 K for 8 h followed by a second heating treatment at 1123 K for 12 h in pellet form. The obtained product was reground and pelletized and again heated at 1173 K for 12 h. The final product was characterized by powder XRD confirming that $InVO_4$-III was the only phase present in the synthesized sample.

Two series of HP XRD experiments were performed: one up to 23.9 GPa and another up to 6.4 GPa. The second experiment was constrained to the pressure stability of orthorhombic phase III (*Cmcm*) and was used to study more accurately the bulk and axial compressibility of it. We used 16:3:1 methanol-ethanol-water as pressure-transmitting medium (PTM). Angle-dispersive XRD experiments were carried out using diamond-anvil cells (DAC) with diamond culets of 300 μm. The pressure chamber was a 100 μm hole drilled on a 40 μm pre-indented inconel gasket. XRD experiments were performed at the MSPD beamline at ALBA synchrotron facility [26]**.** The beamline is equipped with Kirkpatrick-Baez mirrors to focus the monochromatic beam to 20 μm x 20 μm and a Rayonix CCD detector with a 165 mm diameter of active area. We used a wavelength of 0.4246 Å and the sample-detector distance was set to 280 mm. The two-dimensional diffraction images were integrated with FIT2D software [27]**.** Pressure was determined by using Cu as pressure standard [28]. Structural analysis was performed with PowderCell [29] and GSAS [30]. Drawings of crystal structures and calculations of bond distances were carried out using Vesta [31].

Raman studies were performed using small grains of a compacted pellet loaded inside the DAC with 16:3:1 methanol-ethanol-water as PTM. Measurements were carried out in backscattering geometry with a Jobin-Yvon single spectrometer equipped with an edge filter and a thermoelectric-cooled multichannel CCD detector. In these experiments we used ruby florescence for pressure calibration. Measurements with a spectral resolution below 2 cm^{-1} were performed using the 514.5 nm line of an Ar laser. A second set of experiments was conducted using the 488 nm line giving identical results. Laser power was keep below 20 mW to minimize sample heating. Laser power reduction to less than 6 mW does not produce other change than intensity reduction in the Raman spectra confirming than sample heating did not affect our experiments.

3. Results and Discussion

Powder XRD data of the prepared samples were in agreement with the data reported earlier for orthorhombic $InVO_4$ [10,14] and no unaccounted reflection questions its phase purity. The determined unit-cell parameters at ambient pressure are a = 5.761(5) Å, b = 8.530(8), and c = 6.593(6) Å. Pieces of pellets of this characterized sample were used for HP studies. XRD patterns collected at selected pressures are depicted in Fig 1. The powder XRD patterns of the

sample recorded inside the DAC show the distinct reflections due to $InVO_4$ (orthorhombic phase III) and Cu used as pressure maker (indicated by the vertical ticks at the bottom of the diffractogram shown at 0.8 GPa). In addition a broad peak at $2\theta = 12^o$, due to the inconel gasket (marked in Fig 1), is observed in all XRD patterns. The presence of this peak is due to the tail of the X-ray beam (No clean-up pinhole was used in the experiments).

A comparison of the powder XRD patterns recorded at different pressures indicates that the patterns up to 6.2 GPa are almost similar to that observed for ambient pressure orthorhombic $InVO_4$-III. Only a shift towards large angles is observed in the Bragg peaks due to the unit-cell contraction caused by compression. However, the pattern recorded at 6.2 GPa shows several additional weak reflections (most notorious new reflections are indicated by asterisks "*" in Fig.1). Some of the new reflections become more prominent at higher pressure and reflections of the low-pressure phase disappear. This fact suggests that orthorhombic $InVO_4$ undergoes structural changes beyond 6.2 GPa. All the reflections observed in the XRD pattern recorded at 8.2 GPa, could be accounted to a single phase (that we denoted as phase V) and Cu or gasket. Ticks corresponding to diffraction peaks of this structure are shown in the Fig. 1 at 8.2 GPa. In contrast, the XRD patterns measured at 6.2 and 7.2 GPa cannot be accounted by phase III, phase V or the coexistence of both phases. Therefore, we think that in this limited pressure range there is another phase coexisting with phases III and V. We named this phase as phase IV. According to the intensity of Bragg peaks assigned to each phase, phase IV is a minority phase. Raman experiments supports also this conclusion as we will discuss in section 3.c. From 8.2 GPa to the highest pressure (23.9 GPa) diffraction patterns can be indexed with the structure of phase V. Upon rapid decompression from 23.9 GPa to ambient pressure we obtained a mixture of phases III and V. The reported phase transition occurs together with a color change from yellow to red suggesting an alteration of the electronic properties of $InVO_4$ and a collapse of the band gap to values smaller than 1.9 eV [32].

a. Structure of phases III and V of $InVO_4$

The characterization of the $InVO_4$ phases was further carried out by Rietveld refinement of the powder XRD data. The refinements were carried out only for phases III and V because phase IV was never observed as a pure phase. Therefore the structure of phase IV remains unidentified. For the crystal structure refinement, we have used data recorded with $2\theta < 11.5^o$ to

147 avoid the strong peak overlapping contribution either from Cu or gasket with the $InVO_4$ phases.
148 Therefore we have only 14 Bragg peaks for phase III. This phase could be successfully refined
149 with the reported structural details of the orthorhombic $InVO_4$ phase [In: (4a: 0, 0, 0), V: (4c:
150 0,*y*,1/4), O_1: (8g: *x,y,*1/4), and O_2: (8f*:* 0,*y,z*)*,* Z = 4 and SG *Cmcm*]. Since the occupancy and the
151 atomic displacement factors are correlated and more sensitive to background subtraction than
152 positional parameters [33], the occupancies of all atoms were constrained to 1 as established by
153 stoichiometry and results obtained from the experiment made outside the DAC. In order to
154 reduce the number of free parameters in the refinement, the isotropic displacement parameters
155 (B) were also not refined and they were constrained to 0.5 $Å^2$ for all atoms [33]. The scale factor,
156 profile, and unit-cell parameters were first refined and subsequently the position coordinates
157 were refined. The refinement R-factors and structural parameters are given in Table 1. The
158 Rietveld refinement plot for phase III at 0.8 GPa is shown in Fig. 2. The obtained structural
159 parameters at 0.8 GPa resemble closely the values reported in literature [10,14] and found by us
160 at ambient pressure. At 0.8 GPa we found that, within the accuracy of experiments, the atomic
161 positions do not change from those determined at ambient pressure. The structure of phase III
162 has In atoms in nearly regular octahedral coordination with the In-O bonds at 0.8 GPa as: In-O_2
163 2.1483(6) Å (x2) and In-O_1 2.1623(6) Å (x4). The V-O bonds of the tetrahedral VO_4 groups are
164 V-O_1 1.7983(5) Å (x2) and V-O_2 1.6579(5) Å (x2). The distortion from perfect regular polyhedra
165 is similar to that previously reported at ambient pressure [10,14].

166 Due to the above mentioned reason, we used the XRD data recorded below 11.5° for the
167 analysis of HP phase V. The total of 17 reflections observed for this phase in the diffraction
168 pattern recorded at 8.2 GPa could be successfully indexed on a monoclinic lattice. A comparison
169 of the obtained lattice parameters with those of other ABO_4 compounds reported in the literature
170 suggests close proximity with the wolframite-type cell. The calculated Bragg positions are
171 indicated by vertical marks below the diffraction pattern at 8.2 GPa (Fig.1). Other structures like
172 monazite-type, zircon-type, and scheelite-type were also considered but they could not account
173 the position and intensity of the Bragg reflections observed for the HP phase V. Also, the
174 intensity could not be accounted by any of the monoclinic subgroups of space group *Cmcm*. In
175 addition, the symmetry and structural details reported for monoclinic $InVO_4$ (phase I, *C2/m*),
176 prepared at a low temperature solution process, could not account the reflections and intensity of
177 the observed XRD pattern. Disordered rutile-type and α-PbO_2-type structures proposed for the

high pressure-high temperature (HT) structures of $FeVO_4$ and $CrVO_4$ [24] are not compatible with the XRD patterns measured for phase V. In contrast, the intensities of the Bragg reflections could be accounted by a wolframite-type lattice (SG *P2/c*). In addition, an analysis of systematic extinctions is consistent with the assignation of *P2/c* (or a subgroup of it) as the space group. Further the powder XRD pattern collected at 8.2 GPa was refined by the Rietveld method. In the refinement we used the presently obtained unit-cell parameters as starting values. For the crystalline structure we employed a model based on the reported positional coordinates for a wolframite-type structure [22, 34] [In: (2f*: 1/2, y,* 1/4*)*, V: (2e*: 0, y,* 1/4), O_1: (4g*: x, y ,z*), and O_2: (4g*: x, y, z),* Z = 2 and SG *P2/c*). Similar to the analysis of the XRD data of phase III, the occupation and displacement parameters of all the atoms of the HP phase (phase V) were fixed at 1 and 0.5 $Å^2$, respectively. These parameters were not refined in order to restrict the number of free parameters as well as to avoid correlation with the position coordinates of various atoms. Appreciably good match in intensity and profile could be obtained with this refinement as can be seen from Fig 2. The refined unit-cell parameters for the phase V at 8.2 GPa are: a = 4.714(5) Å; b = 5.459(6) Å, c = 4.903(5) Å, and β = 93.8(3)º, V = 125.89(2) $Å^3$. The details of the refined atomic coordinates of phase V are included in Table 1. We would like to mention here that the residuals of the refinement can be minimized when reducing the symmetry of the monoclinic wolframite structure to that of the triclinic subgroup $P\bar{1}$. The transformation from the parent monoclinic to the daughter triclinic structure implies that all atoms will be located at Wyckoff position 2i [In: (1/2, 0.711, 1/4), V: (0, 0.159, 1/4), O_1: (0.214, 0.861, 0.491), O_2: (0.786, 0.861, 0.492), O_3: (0.242, 0.407, 0.399), and O_4: (0.758, 0.407, 0.101)]. In the triclinic distorted-wolframite structure, the α and γ angles are free parameters. The "best" structural refinement (R_P = 5.23 % and R_{WP} = 6.85 %) is found for α = γ = 90.2(1)º with the rest of the structural parameters being the same that in monoclinc wolframite. Unfortunately, the limited angular range used for the structural refinement does not allow a clear discrimination between both structures, which becomes even more difficult as pressure increases. However, both structures can be described as wolframite-type structures [34,35]. The main difference between them is the lost of the binary screw axis parallel to the crystallographic *b*-axis when reducing the symmetry from *P2/c* to $P\bar{1}$.

The crystal structure of phases III and V of $InVO_4$ are shown in Fig. 3. A comparison of the structures of $InVO_4$-III and $InVO_4$-V suggests the structural transition is of first-order and

209 reconstructive type. It involves a large volume collapse ($\Delta V/V$ = -14%). The analyses of the
210 structural parameters revealed that vanadium atoms have octahedral coordination with larger
211 dispersion in the V-O bond lengths. The observed V-O bond lengths in phase V at 8.2 GPa are:
212 V-O_1 1.6730(5) Å (x2), V-O_2 1.8861(5) Å (x2), and V-O_1 2.2166(6) Å (x2). In contrast, the
213 observed bond lengths in the InO_6 polyhedra indicate a less distorted octahedron [In-O_2 2.2101(6)
214 Å (x2), In-O_2 2.1397(6) Å (x2), and In-O_1 2.0268(6) Å (x2)], which however is more distorted
215 than the equivalent octahedron in phase III. According to the above described structure of phase
216 V, the phase transition is accompanied by a change in the coordination sphere around vanadium
217 (tetrahedral to octahedral) without any drastic change with respect to the octahedral coordination
218 of indium. It may also be noted that the monoclinic lattice of phase I has all the vanadium atoms
219 in tetrahedral coordination. As mentioned in the introduction section, $InVO_4$ shows a rich crystal-
220 chemistry and can exist in different structure types depending on the method and temperature of
221 preparation. In both phase I and III, the In and V atoms have octahedral and tetrahedral
222 coordination, respectively, and also have closely similar arrangements of the InO_6 and VO_4 units.
223 In between phase I and III of $InVO_4$, the existence of an intermediate phase II is reported in
224 literature [11,12]. However, the details of the crystal structure of this phase II are not known due
225 to its limited stability and irreproducibility in preparation. As phase II is formed in between the
226 transition from phase I to III, no increase in coordination number of vanadium is expected in this
227 structure. The present observation thus claimed as the first known polymorph of $InVO_4$ with
228 octahedrally coordinated vanadium atoms, which is obtained only by the application of pressure.
229 Previously, a disordered wolframite-type structure, with possible vanadium six-fold coordinated,
230 has been obtained in related vanadates but applying HP and HT simultaneously [24]. However,
231 for this structure the atomic positions are not reported, and therefore the vanadium coordination
232 is unknown.

233 Recently, first-principle calculations predicted that a $CrVO_4$-type to wolframite-type
234 structural transition is energetically favored in $InPO_4$ structure above 47 GPa [22]. Since
235 phosphorous in octahedral coordination has been limited by crystallography, due to its small
236 ionic radius, only a few examples of six-coordinated phosphorous are known. Usually, they have
237 been found at extremely high pressure [21]. However, such examples (octahedral B site cation)
238 are commonly observed in tungstates or molybdates [36-38]. High pressure and/or temperature
239 studies on tungstates indicate that the conversion from tetrahedral WO_4 to octahedral WO_6 is

favored by phase transitions. Since vanadium can sustain a wider coordination number, namely 4, 5 and 6 one can easily expect an increase in coordination number under pressure compared to analogous phosphates. Indeed, the present results suggest that structures with six-coordinated vanadium can be obtained in $CrVO_4$-type vanadates at relative low pressure (< 10 GPa). In the case of $InVO_4$, the presence of six-coordinated vanadium may lead to maximum efficiency for the splitting of water molecules by visible light [7], opening the door to novel technological applications.

b. Pressure evolution of unit-cell parameters and equation of state

The pressure evolution of the unit-cell parameters of phases III and V were studied from the XRD patterns recorded at different pressures. To reduce the number of parameters, the HP phase was described as the monoclinic wolframite phase (SG *P2/c*). The evolution of phases and transition were concluded by comparing XRD patterns of successive pressures. As mentioned earlier, the diffraction patterns recorded up to 6.2 GPa all can be attributed to orthorhombic $InVO_4$ (phase III) and at 8.2 GPa and beyond they correspond to phase V. Among the measured HP XRD data, it is observed that XRD patterns from 6.2 to 7.2 GPa have contributions from the coexisting phases III, IV, and V. For the low-pressure phase, all the reflections are well defined for every pressure. Given the pressure range of stability of this phase, experimental conditions can be considered as quasi-hydrostatic (deviatoric stresses are negligible) [39,40]. This is observed in the two experiments carried out for phase III. Peaks observed for the HP phase V are slightly broadened under compression, but shape and width of peaks suggest that the deviatoric stresses do not influence much the XRD patterns [41]. Thus, unit-cell parameters of phase V could be accurately followed up to 23.9 GPa. All the XRD patterns were indexed for the assigned phases and subsequently refined using the atomic positions details obtained from the data at 0.8 GPa (for phase III) and 8.2 GPa (for phase V). We found that, within the pressure range of the experiments, in the low-pressure phase, the change of atomic positions are comparable with the experimental uncertainty. Therefore, we concluded that the pressure effect on the atomic positions can be neglected for phase III. Since large uncertainties are obtained for atomic positions in phase V (due to peak broadening as pressure increase) we assume the same hypothesis for it.

The refined unit-cell parameters and volume of phases III and V at different pressures are shown in Fig 4. In the low-pressure phase, the pressure evolution of the volume is well described by a second-order Birch-Murnaghan (BM) equation of state (EOS) with V_0 = 324.0(9) Å^3 and B_0 = 69(1) GPa (B_0' = 4), where V_0 is the unit-cell volume at ambient pressure, B_0 the bulk modulus, and B_0' its pressure derivative. The reduced chi-square value for the fitting was 0.997. In the figure, in addition to the experimental data (circles and squares depending upon experiment) we show the result of the 2nd order EOS as a solid line. It can be seen from Fig. 4, that the axial compressibilities of phase III are highly anisotropic with the smallest compression along the *a*-axis compared to *c*- and *b*-axes. This fact is consistent with the distinctive pressure evolution of (200), (020), and (002) Bragg peaks in Fig. 1, where the larger shift of (020) peak towards higher angles is evident in accordance with the fact that the *b*-axis is the most compressible axis. This can be expected from the arrangement of the InO_6 and VO_4 polyhedra in the unit cell. The anisotropic compression can be related with the fact that there are not VO_4 tetrahedra in between the InO_6 octahedra along the *b*-axis direction. Assuming atomic positions do not change significantly with pressure, we observed that V-O_1 and V-O_2 bonds have similar compressibility for phase III. At 7.2 GPa the V-O_1 and V-O_2 bond distances are 1.735(1) and 1.603(1) Å, respectively. In contrast in the InO_6 octahedra of phase III, the observed long equatorial distance show a similar compressibility than the V-O distances, but the short axial In-O_2 distance is much more compressible than the other bond distances. At 7.2 GPa In-O_1 and In-O_2 bonds are 2.131(1) and 2.033(1) Å, respectively. Note that from 0.8 to 7.2 GPa the In-O_2 bonds are reduced by 6%, whereas the reduction of other bonds is around 2%. Therefore, the distortion of InO_6 octahedra is enhanced under compression. The change of the distortion of VO_4 tetrahedra under compression is less important. In the literature, there are several parameters used as a measure of the grade of distortion in coordination polyhedra [35,42]. In this work we use the distortion parameter Δ_d defined as:

$$\Delta_d = \left(\frac{1}{n}\right)\sqrt{\sum_{1}^{n}\left[\frac{d_i - d}{d}\right]^2} \quad ,$$

where d is the average In-O (V-O) bond distance, d_i are the individual In-O (V-O) bond distances, and n = 6 (4) for the octahedron (tetrahedron). For the InO_6 octahedron Δ_d increases from 1 × 10^{-3} at the lowest measured pressure to 9 × 10^{-3} at 7.2 GPa (9 times). For the VO_4

tetrahedron, within the same pressure interval, Δ_d increases from 2.1×10^{-2} to 2.4×10^{-2} (only 1.14 times). As mentioned earlier, the InO_6 octahedra are connected by sharing the edges forming a linear chain of octahedral units along the *c*-axis while the chains are linked by VO_4 by sharing only the corners. The high compressible axis of the InO_6 octahedra, corresponding to the In-O_2 bonds, is aligned along the *b*-axis. Since these bonds are more compressible than equatorial bonds, the InO_6 octahedra are flattened upon compression. Thus, it is reasonable to have the largest axial compressibility along *b*-axis.

The pressure evolution of unit-cell parameters can be well described with the following linear equations:

$$a\ (\text{Å}) = 5.761(2) - 4.5(7) \times 10^{-3}\ \text{P}$$

$$b\ (\text{Å}) = 8.542(9) - 7.2(3) \times 10^{-2}\ \text{P}$$

$$c\ (\text{Å}) = 6.593(6) - 2.4(2) \times 10^{-2}\ \text{P}$$

where the pressure P is in GPa. The ambient pressure axial compressibilities (defined for a given dimension x as $\kappa_x = -\frac{\partial \ln x}{\partial P}$) are: $\kappa_a = 7.8 \times 10^{-4}$ GPa^{-1}, $\kappa_b = 8.5 \times 10^{-3}$ GPa^{-1}, and $\kappa_c = 3.6 \times 10^{-3}$ GPa^{-1}.

From the analyses of the bond lengths, it is seen that local coordination around the vanadium atom change significantly after the phase transition. For the VO_6 polyhedra, at 8.2 GPa the two short V-O distances are in average 7 % longer than the average distances at 7.2 GPa in the VO_4 tetrahedron. However, two extra bonds, which are more than 0.32 Å longer than the other V-O distances, are added to form a highly distorted VO_6 octahedron. The enlargement of the average V-O bond distances is in agreement with the coordination increase of the V atoms. Compared to the InO_6 octahedron, the VO_6 units are highly distorted. Further, it can be noted that at the phase transition the In-O distances are much less modified than then V-O distances (the agreement is within 3 % when comparing phase III at 7.2 GPa with phase V at 8.2 GPa). An analysis of the pressure dependent unit-cell parameters of the phase V indicates that the *b*-axis is the most compressible one and the *a*-axis is highly incompressible. Furthermore, the unit-cell parameters show non-linear compressibility in phase V and the pressure dependent unit-cell parameters could be fitted by 2nd order polynomial equations as below.

326 a (Å) $= 4.720(4) - 7.5(4) \times 10^{-4}\,P + 5.3(4) \times 10^{-6}\,P^2$

327 b (Å) $= 5.650(5) - 2.6(1) \times 10^{-2}\,P + 3.4(3) \times 10^{-4}\,P^2$

328 c (Å) $= 4.950(4) - 6.0(3) \times 10^{-3}\,P + 5.4(4) \times 10^{-5}\,P^2$

329 β (º) $= 92.4(5) + 0.164(6)\,P - 1.87(8) \times 10^{-3}\,P^2$

330 where P is the pressure in GPa.

331 In Fig. 4 we compare the unit-cell volume vs. pressure behavior obtained for phases III
332 and V. In order to facilitate the comparison we doubled the volume of the HP phase. The
333 pressure evolution of the volume of phase V can be described with a 2nd order BM EOS. The
334 EOS parameters are V_0 = 131.6(6) Å^3 and B_0 = 168(9) GPa (B_0' = 4). The reduced chi-square
335 value for the fitting was 0.993. It is observed that the bulk modulus for the phase V is nearly
336 three times that of the low-pressure phase. This is consistent with the large volume collapse
337 associated with the phase transition and with the fact that the HP phase is much denser that the
338 low-pressure phase (void space between polyhedra is reduced), which is consistent with the
339 coordination number increase of vanadium. Also the value of B_0 = 168(9) is comparable with
340 that of AVO_4 scheelite-type and zircon-type vanadates [43]. In the latter structures compression
341 is coming from the reduction of A-O distances. An empirical model has been developed to
342 estimate the bulk modulus for zircon and scheelite oxides [15]. It has been proved to work well
343 also in other ABO_4 structures [34,44], in particular wolframites. According to this model:

344 $$B_0 = (610 \pm 110)\frac{Z_{In}}{d_{In-O}^{\ 3}}$$

345 where B_0 is the bulk modulus (in GPa), Z_{In} is the In formal charge, and $d_{In\text{-}O}$ is the average In-O
346 distance (in Å) inside the InO_6 octahedron at ambient pressure. In-O distances cannot be obtained
347 accurately for the wolframite phase at ambient pressure because on pressure release we
348 recovered a mixture of phases. To estimate them, we extrapolated the unit-cell parameters and
349 assumed the atomic positions do not change with pressure. We got B_0 = 180(30) GPa. This value
350 (an upper limit for B_0 because in the empirical model V-O distances are assumed to be rigid and
351 not to contribute to volume reduction) shows that the value obtained from our EOS is reasonable.
352 Note that a similar increase in bulk modulus is found in $AlPO_4$ when phosphorous coordination
353 is increased from 4 to 6 [21].

c. Raman spectroscopy

HP Raman spectra recorded for $InVO_4$ are shown in Fig. 5. We also collected Raman spectra at ambient conditions. They resemble the one measured at 0.3 GPa and those spectra reported earlier [45,46]. According to group theory, the orthorhombic low-pressure phase has fifteen Raman-active modes with symmetries: $\Gamma = 5\ A_g + 4\ B_{1g} + 2\ B_{2g} + 4\ B_{3g}$ [45]. We have found the fifteen modes, while previously only six modes were reported [45]. Out of them, five agree with our results with a frequency difference of less than 1 %. The remaining mode reported in Ref. [45] at 404 cm^{-1} is detected in our experiments at 390 cm^{-1}. The observed Raman modes are given in Table 2 and compared with Ref. [45]; pressure coefficients are also given. Fig. 6 presents the pressure evolution of Raman modes. It can be seen there that all modes shift to higher frequency upon compression. The pressure variations of mode frequencies can be described with a linear function. The modes at high frequency are attributed to internal modes of tetrahedral VO_4 groups [45], being the mode observed at 918 cm^{-1} the strongest one. We found that the fifteen Raman modes harden upon compression. The modes labelled as ω_6, ω_{10}, ω_{11}, and ω_{12} have the largest pressure coefficients. One of them (ω_{12}) corresponds to an internal stretching mode of the VO_4 tetrahedron [22,45]. The other stretching mode, ω_{15}, is also more sensitive to pressure than the bending modes of the VO_4 tetrahedron (ω_5 and ω_9). In particular, the mode at 342 cm^{-1} is the mode less affected by pressure.

In Fig. 5 it can be seen that at 3.8 GPa, subtle changes develop in the Raman spectrum. Additional changes occur up to 8.8 GPa. They are indicative of the occurrence of phase transitions. In particular, as in XRD experiments, we identified the presence of two HP phases, both appearing at 3.8 GPa. However, phase III can be identified as the predominant phase up to 6.4 GPa. Regarding the HP phases, one of them can be identified with phase V remaining stable up to the highest pressure covered by the experiments. At 8.8 GPa and beyond, phase V is found as a single phase as in XRD. The other phase coexists with phases III and V and its presence is consistent with the detection of phase IV by XRD. Phase IV is a minority phase up to 7 GPa. The pressure-released Raman spectrum indicated the coexistence of phases III and V at ambient pressure. All these conclusions fully agree with the picture extracted from XRD experiments.

The pressure evolution of the Raman modes identified for phases IV and V is shown in Fig. 6. Raman frequencies at 7 GPa and pressure coefficients are summarized in Table 3. In

384 phase V we identified eighteen Raman modes and in phase IV eight modes. Regarding pressure
385 coefficients, in phases IV and V all of them are positive, with the exemption of the coefficients
386 of ω_1 in phase IV and ω_4 and ω_7 in phase V which are basically not affected by pressure.

387 We will focus now the discussion of Raman on phase V, leaving the systematic study of
388 phase IV to a future research. For a monoclinic wolframite structure (*P2/c*), group theory
389 predicts eighteen Raman active modes: $\Gamma = 8\ Ag + 10\ Bg$. For the triclinic wolframite ($P\bar{1}$) the
390 same number of modes is expeccted, but all of them are Ag modes. For phase V we have
391 detected 18 modes, which support the assignation of phase V to a wolframite-type structure. In
392 addition, the Raman spectra of phase V resemble those of wolframite-type tungstates [47,48]. In
393 particular, the presence of four high-frequency modes (see Table 3) separated by a phonon gap
394 from the rest of the modes is a typical feature of wolframite. Another distinctive fact of
395 wolframites is that the mode observed near 900 cm^{-1} (850 cm^{-1} in phase V) is the most intense
396 mode as we found (see Fig. 5). Finally, the abrupt decrease of the frequency of the highest
397 frequency mode in phase V in comparison with phase III is consistent with the increase of the
398 CN and the V-O bond lengths. As a consequence of it, the bond strength is expected to decrease
399 [49], hence the mode frequency drops, as observed in the high-frequency modes associated to
400 internal stretching modes in wolframite-type oxides [50,51]. Based upon all these facts, we
401 conclude that Raman experiments support the structural assignation made from XRD.

402 Raman experiments can provide a hint for the distinction between the monoclinic and
403 triclinic wolframite structures. Selection rules state that Bg modes should disappear with parallel
404 polarization. We performed polarized Raman scattering measurements and found that all modes
405 are present for parallel polarization, which supports that phase V has the triclinic structure.
406 However, we prefer to be cautious and leave the definitive answer to future studies because it is
407 know that in DAC experiments selection rules could be “apparently violated” by the lack of
408 polarization in the DAC or the possible appearance of structural defects.

409 To conclude, we would like to mention that in Raman experiments we also observed the
410 color change detected in XRD experiments at the III-to-V transition. This change suggests a
411 decrease of the band-gap energy, being it consistent with the band-gap collapse observed at
412 pressure-induced transitions in rare-earth orthovanadates [50,51].

413

4. Conclusions

We presented results of *in situ* high-pressure XRD and Raman studies on orthorhombic $InVO_4$ and reported a new phase with octahedral coordinated vanadium atoms. The crystal structure of the HP phase has been elucidated as a distorted wolframite-type having ordered arrangement of InO_6 and VO_6 polyhedral units. The observed new phase is the first known cation-ordered phase of $InVO_4$ having vanadium atoms in six coordination. These results are in accordance with the recently predicted $CrVO_4$-type to wolframite-type HP transition in related phosphates. The high-pressure phase is relatively incompressible as indicated by a large bulk modulus. The low-pressure phase is much more compressible. In both structures compression is highly anisotropic. Raman spectroscopy confirms the conclusions extracted from XRD measurements. These measurements also allowed the identification of all Raman-active modes in the low- and high-pressure phase as well as their pressure coefficients. These results indicate a new room-temperature structural transition sequence in the $CrVO_4$-type orthovanadates and are useful to understand lattice-dynamics properties of orthovanadates. The new phase of $InVO_4$ has apparently a smaller band gap that the already known phases, which could be useful for the development of applications like photocatalytic hydrogen production [7].

AUTHOR INFORMATION

Corresponding Author

*E-mail: daniel.errandonea@uv.es

Author Contributions

The manuscript was written through contributions of all authors. All authors have given approval to the final version of the manuscript.

Notes

The authors declare no competing financial interests.

ACKNOWLEDGMENT

Research supported by the Spanish government MINECO under Grants No.: MAT2010-21270-C04-01/04 and CSD2007-00045. O. Gomis thanks the support from Vicerrectorado de Investigación y Desarrollo of UPV (Grants No.: UPV2011-0914 PAID-05-11 and UPV2011-

0966 PAID-06-11). S. N. Achary acknowledges the support provided by Universitat de Valencia during his visit to it. B. G.-D. acknowledges the financial support from MINECO through the FPI program.

REFERENCES

(1) Baran E. J. *J. Mater. Sci.* **1998**, *33*, 2479.

(2) Ai, Z; Zhang, L; Lee, S. *J. Phys. Chem. C* **2010**, *114,* 18594.

(3) Enache, C. S.; Lloyd, D.; Damen, M. R.; Schoonman, J.; van de Krol, R. *J. Phys. Chem. C.* **2009**, *113,* 19351.

(4) Lin, H. Y.; Chen, Y. F.; Chen, Y. W. *Int. J. Hydrogen Energy* **2007***, 32***,** 86.

(5) van de Krol, R.; Śegalini, J.; Enache, C. S. *J. Photonics Energy,* **2011***, 1*, 016001.

(6) Butcher, Jr. D. P.; Gewirth, A. A. *Chem. Mater.* **2010**, *22*, 2555.

(7) Zou, Z.; Ye, J.; Sayama, K.; Arakawa, H. *Nature* **2001**, *414*, 625.

(8) Orel, B.; Šurca Vuk, A.; Opara Krašvec, U.; Drazic, G. *Electrochim. Acta* **2001***, 46*, 2059.

(9) Denis, S.; Baudrin, E.; Touboul, M.; Tarascon, J. M. *J. Electrochem. Soc*. **1997**, *144*, 4099.

(10) Touboul, P.M.; Toledano, P. *Acta. Cryst. B*. **1980**, *36*, 240.

(11) Touboul, P.M.; Melghit, K. *J. Solid State Chem*. **1995**, *118***,** 93.

(12) Touboul, P.M.; Ingrain, D.; *J. Less Common Metal*. **1980**, *71***,** 55.

(13) Roncaglia, D. I.; Botto, I. L.; Baran, E. J. *J. Solid State Chem*. **1986**, *62*, 11.

(14) Katari, V.; Patwe, S. J.; Achary,S. N.; Tyagi, A. K. *J. Am. Ceram. Soc.* **2013***, 96,* 166.

(15) Errandonea,D.; Manjón, F. J. *Prog. Mater. Sci*. **2008**, *53*, 711.

(16) Errandonea, D.; Gracia, L.; Beltrán, A.; Vegas, A.; Meng, Y. *Phys. Rev. B* **2011**, *84*, 064103.

(17) Errandonea, D.; Kumar, R.; López-Solano, J.; Rodríguez-Hernández, P.; Muñoz, A.; Rabie, M. G.; Sáez Puche, R. *Phys.Rev. B* **2011,** *83*, 134109.

(18) Kanzaki, M.; Xue, X.; Reibstein, S.; Berryman, E.; Namgung, S. *Acta Cryst. B* **2011**, *67*, 30.

(19) Manjón, F.J.; Errandonea, D. *Phys. Stat. Solidi B* **2009,** *246*, 9.

(20) Sharma, S. M.; Garg, N.; Sikka, S. K. *Phys. Rev. B* **2000**, *62*, 8824.

(21) Pellicer-Porres, J.; Saitta, A. M.; Polian, A.; Itie, J. P.; Hanfland, M. *Nature Mater.* **2007,** *6*, 698.

(22) Lopez-Moreno,S.; Errandonea, D. *Phys, Rev. B* **2012**, *86*, 104112.

(23) Young,A. P.; Schwartz, C.M. *Acta Cryst.* **1962**, *15*, 1305.

(24) Laves, F.; Young, A. P.; Schwartz, C. M. *Acta Cryst.* **1964,** *17*, 1476.

(25) Tojo, T.; Zhang, Q.; Saito, F. *J. Solid State Chem*. **2006,** *179*, 433.

(26) Knapp, M.; Peral, I.; Nikitina, L.; Quispe, M.; Ferrer, S. *Z. Kristallogr. Proc.* **2011**, *1*, 137.

(27) Hammersley, A. P.; Svensson, S. O.; Hanfland, M.; Fitch, A. N.; Hausermann, D. *High Press. Res.* **1996**, *14*, 235.

(28) Dewaele, A.; Loubeyre, P.; Mezouar, M. *Phys. Rev. B* **2004**, *70*, 094112.

(29) Kraus,W; Nolze, G. *J. Appl. Crystallogr.* **1996**, *29*, 301.

(30) Larson, A. C.; von Dreele R.B. GSAS: General Structure Analysis System. Los Alamos National Laboratory, Report LA-UR 86-748, **2000**.

(31) Momma, K; Izumi F. *J. Appl. Crystallogr.* **2011**, *44*, 1272.

(32) Bandiello, E.; Errandonea, D.; Martinez-Garcia, D.; Santamaria-Perez, D.; Manjon, F. J. *Phys. Rev. B* **2012**, *85*, 024108.

(33) Gomis, O.; Sans, J. A.; Lacomba-Perales, R.; Errandonea, D.; Meng, Y.; Chervin, J. C.; Polian, A. *Phys. Rev. B* **2012**, 86, 054121.

(34) Ruiz-Fuertes J.; López-Moreno, S.; Errandonea, D.; Pellicer-Porres, J.; Lacomba-Perales, R.; Segura, A.; Rodríguez-Hernández, P.; Muñoz, A.; Romero, A. H.; González, J. *J. Appl. Phys.* **2010**, *107*, 083506.

(35) Ruiz-Fuertes, J.; Friedrich, A.; Pellicer-Porres, J.; Errandonea, D.; Segura, A.; Morgenroth, W.; Haussühl, E.; Tu, C. Y.; Polian, A. *Chem. Mater.* **2011**, 23, 4220.

(36) Errandonea, D.; Somayazulu, M. Häusermann, D. *Phys. Stat. Sol. B* **2002**, *231*, R1.

(37) Achary, S.N.; Mukherjee, G.D.; Tyagi,A.K.;Vaidya, S.N. *J. Mater. Sci.* **2002***, 37*, 2501.

(38) Errandonea, D.; Gracia, L.; Lacomba-Perales, R.; Polian, A.; Chervin, J. C. *J. Appl. Phys.* **2013**, *113*, 123510.

(39) Klotz, S.; Chervin, J. C.; Munsch, P.; Le Marchand, G. *J. Phys. D: Appl. Phys.* **2009**, 42, 075413.

(40) Errandonea, D.; Meng, Y.; Somayazulu, M.; Häusermann, D. *Physica B* **2005**, *355*, 116.

(41) Errandonea, D.; Ferrer-Roca, Ch., Martínez-Garcia, D.; Segura, A.; Gomis, O.; Muñoz, A.; Rodríguez-Hernández, P.; López-Solano, J.;Alconchel, S.; Sapiña, F. *Phys. Rev. B* **2010**, *82*, 174105.

(42) Fleet, M.E. *Mineralogical Magazine* **1976,** *40*, 531.

(43) Errandonea, D.; Lacomba-Perales, R.; Ruiz-Fuertes, J.; Segura, A.; Achary, S.N.; Tyagi, A. K. *Phys. Rev. B* **2009**, *79,* 184104.

(44) Santamaria-Perez, D.; Gracia, L.; Garbarino, G.; Beltrán, A.; Chuliá-Jordán, R.; Gomis, O.; Errandonea, D.; Ferrer-Roca, Ch.; Martínez-García, D.; Segura, A. *Phys. Rev. B* **2011**, *84*, 054102.

(45) Baran, E. J.; Escobar, M. E. *Spectrochim. Acta A.* **1985***, 41,* 415.

(46) Vuk, A. S.; Orel, B.; Drazic,G.; Colomban, P. *Monatsh. Chem.* **2002**, *133*, 889.

(47) Ruiz-Fuertes, J.;.Errandonea, D.; López-Moreno, S.; González, J.; Gomis, O.; Vilaplana, R.; Manjón, F.J.; Muñoz, A.; Rodríguez-Hernández, P.; Friedrich, A.; Tupitsyna, I.A.; Nagornaya, L.L. *Phys. Rev B* **2011**, *83,* 214112.

(48) Ruiz-Fuertes, J.; Errandonea, D.; Lacomba-Perales, R.; Segura, A.; González, J.; Rodríguez, F.; Manjón, F.J.; Ray, S.; Rodríguez-Hernández, P.; Muñoz, A.; Zhu, Z.; Tu, C.Y. *Phys. Rev. B* **2010**, *81*, 224115.

(49) Hofmeister, A.M.; *Phys. Rev. B* 1997, *56*, 5835.

(50) Errandonea, D.; Achary, S.N.; Pellicer-Porres, J.; Tyagi, A.K. *Inorganic Chemistry* **2013**, *52*, 5464.

(51) Panchal, V.; Errandonea, D.; Segura, A.; Rodríguez-Hernandez, P.; Muñoz, A.; Lopez-Moreno, S.; Bettinelli, M. *J. Appl. Phys.* **2011**, *110*, 043723.

526 **Table and figure captions**

527 **Table 1**. Refined crystal structure and bond-length distances of low- (phase III) and high-
528 pressure phase (phase V) of $InVO_4$

529 **Table 2**. Raman frequencies ω_0 (cm^{-1}) of orthorhombic $InVO_4$ at ambient pressure compared
530 with Ref. [45]. The mode assignment of Ref. [45] is given; ν_2 and ν_4 (ν_1 and ν_3): bending
531 (stretching) modes of VO_4 tetrahedron. Pressure coefficients $d\omega/dP$ (cm^{-1}/GPa) are also given.

532 **Table 3**. Raman-mode frequencies ω (cm^{-1}) of phases IV and V of $InVO_4$ at 7 GPa. Pressure
533 coefficients $d\omega/dP$ (cm^{-1}/GPa) are also given.

534 **Figure 1**. Powder XRD patterns of $InVO_4$ at selected pressures. Cu and gasket peaks are
535 identified. Ticks indicate the position of Bragg peaks of phases III and V.

536 **Figure 2**. Rietveld refinement plots for orthorhombic (phase III) and high-pressure (phase V)
537 $InVO_4$. Dots: experiments. Solid lines: refinements. Dashed lines: residuals. Ticks indicate the
538 position of calculated Bragg reflections. The hkl indexing of both phases is also shown.

539 **Figure 3**. Crystalline structure of orthorhombic (left) and wolframite-type (right) $InVO_4$. The
540 coordination polyhedra described in the text are shown. In atoms are shown as large purple
541 spheres, V atom as medium-size red spheres, and O atoms as small red spheres.

542 **Figure 4**. (top) Pressure dependence of unit-cell parameters of orthorhombic and wolframite-
543 type $InVO_4$. The inset shows the pressure evolution of the β angle in the wolframite structure.
544 (bottom) Pressure dependence of the unit-cell volume. Solid symbols: orthorhombic phase.
545 Empty symbols: HP phase. Lines represent the fits and equations of state described in the text.

546 **Figure 5**. Selected high-pressure Raman spectra on $InVO_4$. Numbers on the right indicate
547 pressure in GPa. Symbols at selected features help to identify the stability range of each of the
548 three phases observed. The orthorhombic phase is found from ambient conditions to 6.4 GPa
549 (dollar). The intermediate phase (stars) is detected from 3.8 to 7 GPa. The HP phase (ticks) is
550 observed from 3.8 GPa to the highest pressure attained 16.9 GPa.

551 **Figure 6**. Pressure dependence of phonon wavenumbers as measured by the Raman experiments.
552 Hollow (filled) symbols correspond to the experiment excited with the 514.5 (488) cm^{-1} line.
553 Circles, stars and squares are associated with phases III, IV, and V, respectively.

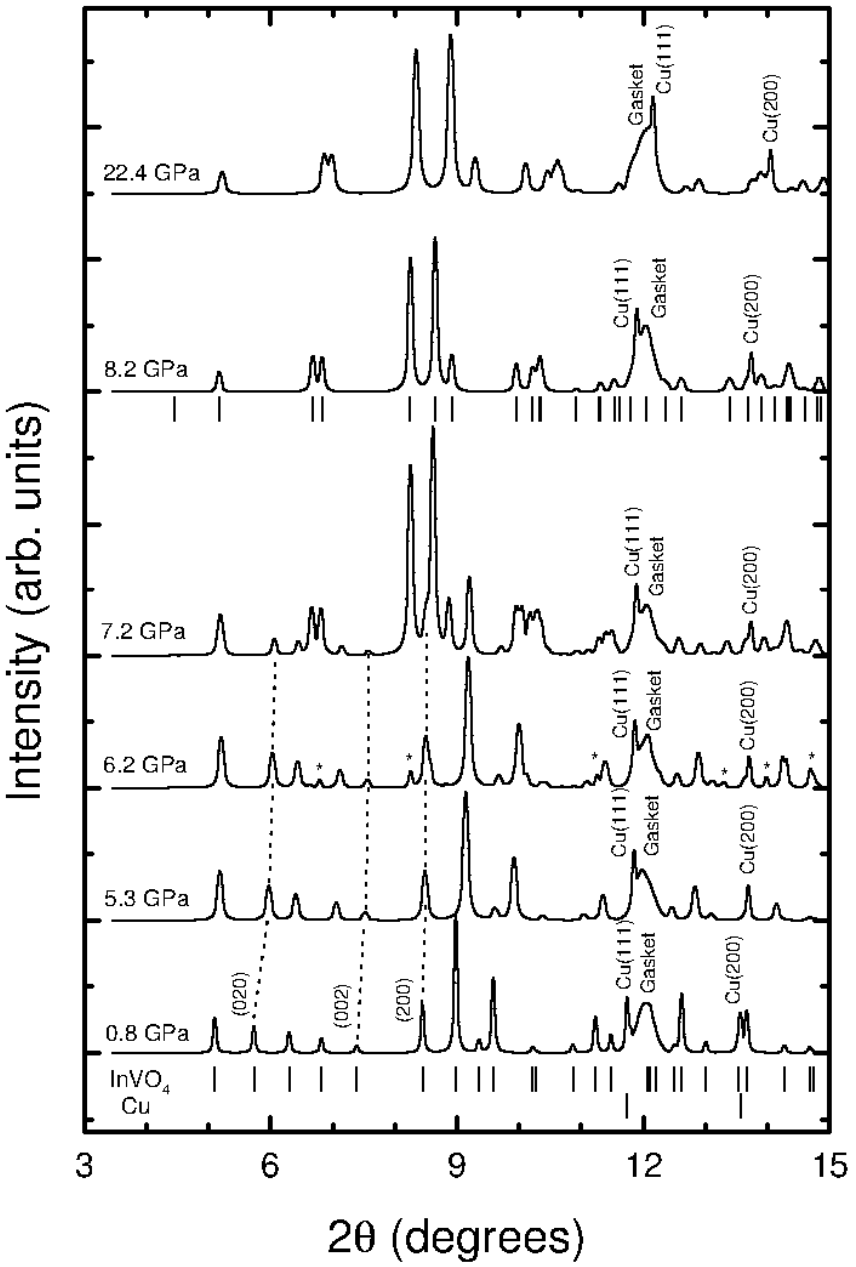
Intensity (arb. units)
2θ (degrees)
3
6
9
12
15
22.4 GPa
8.2 GPa
7.2 GPa
6.2 GPa
5.3 GPa
0.8 GPa
InVO4
Cu
(020)
(002)
(200)
Cu(111)
Gasket
Cu(200)
*

554 **Figure 1**

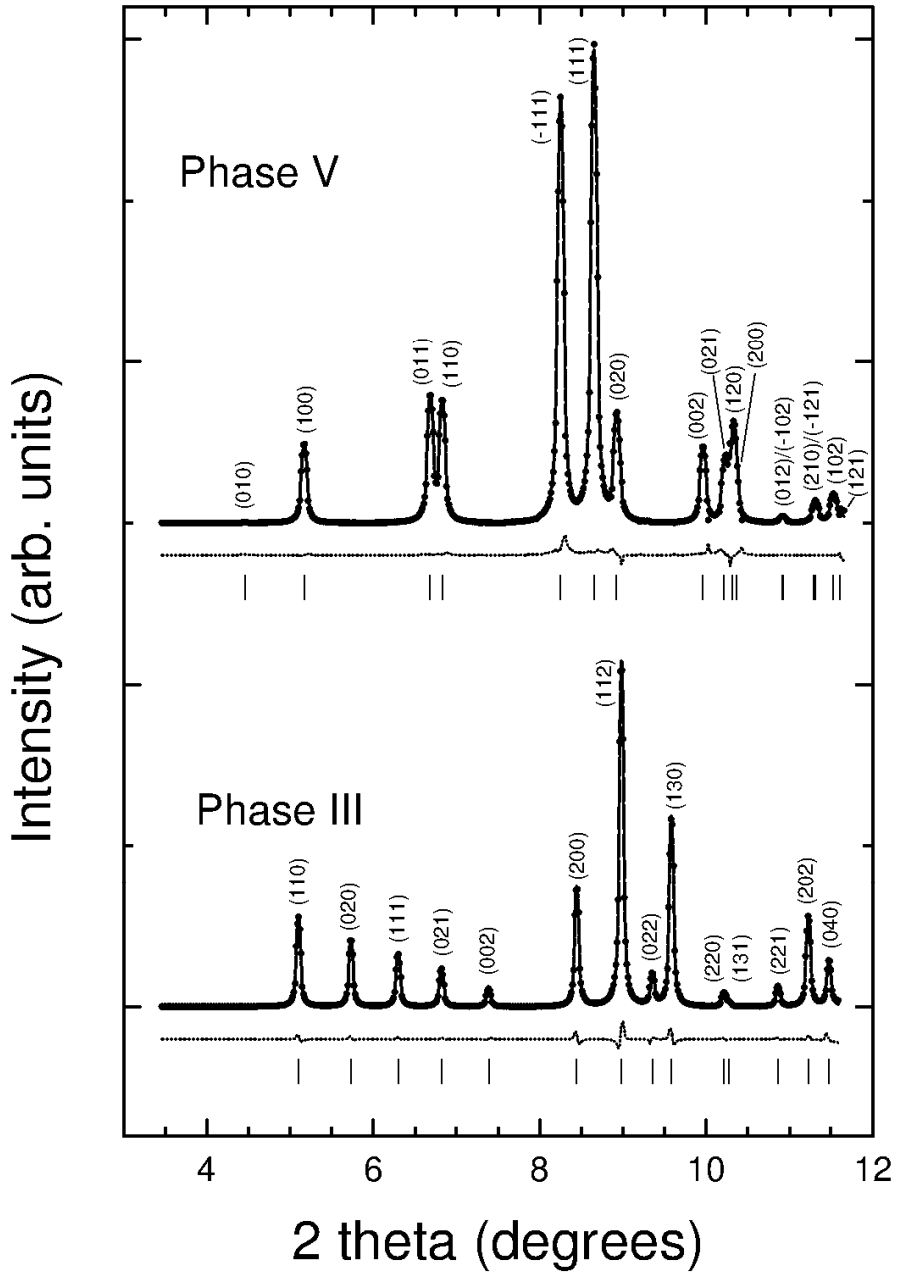

555
556 **Figure 2**

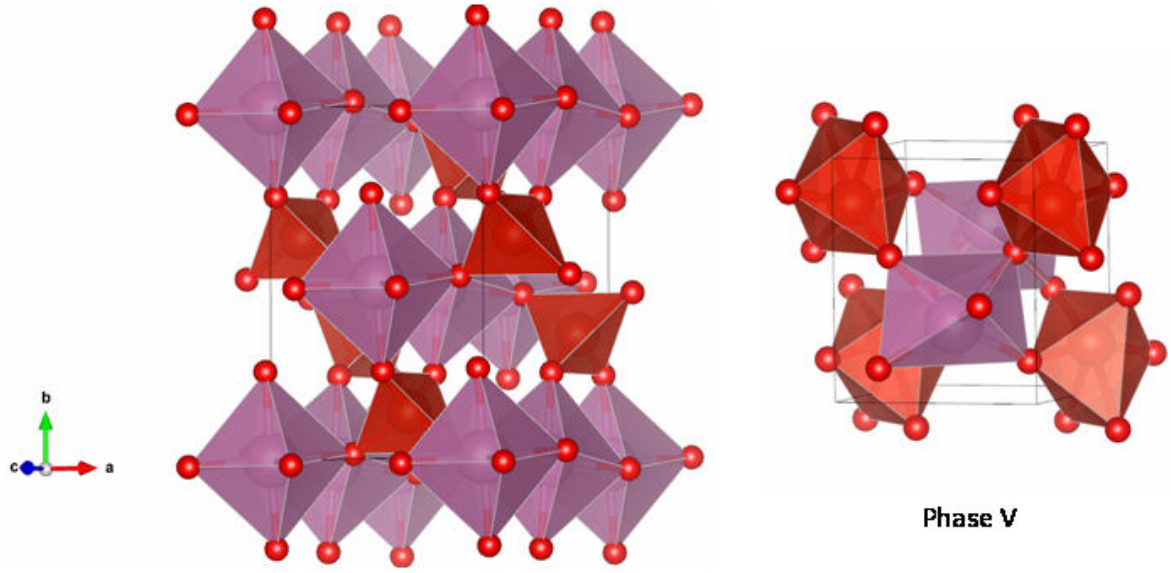

Figure 3

569

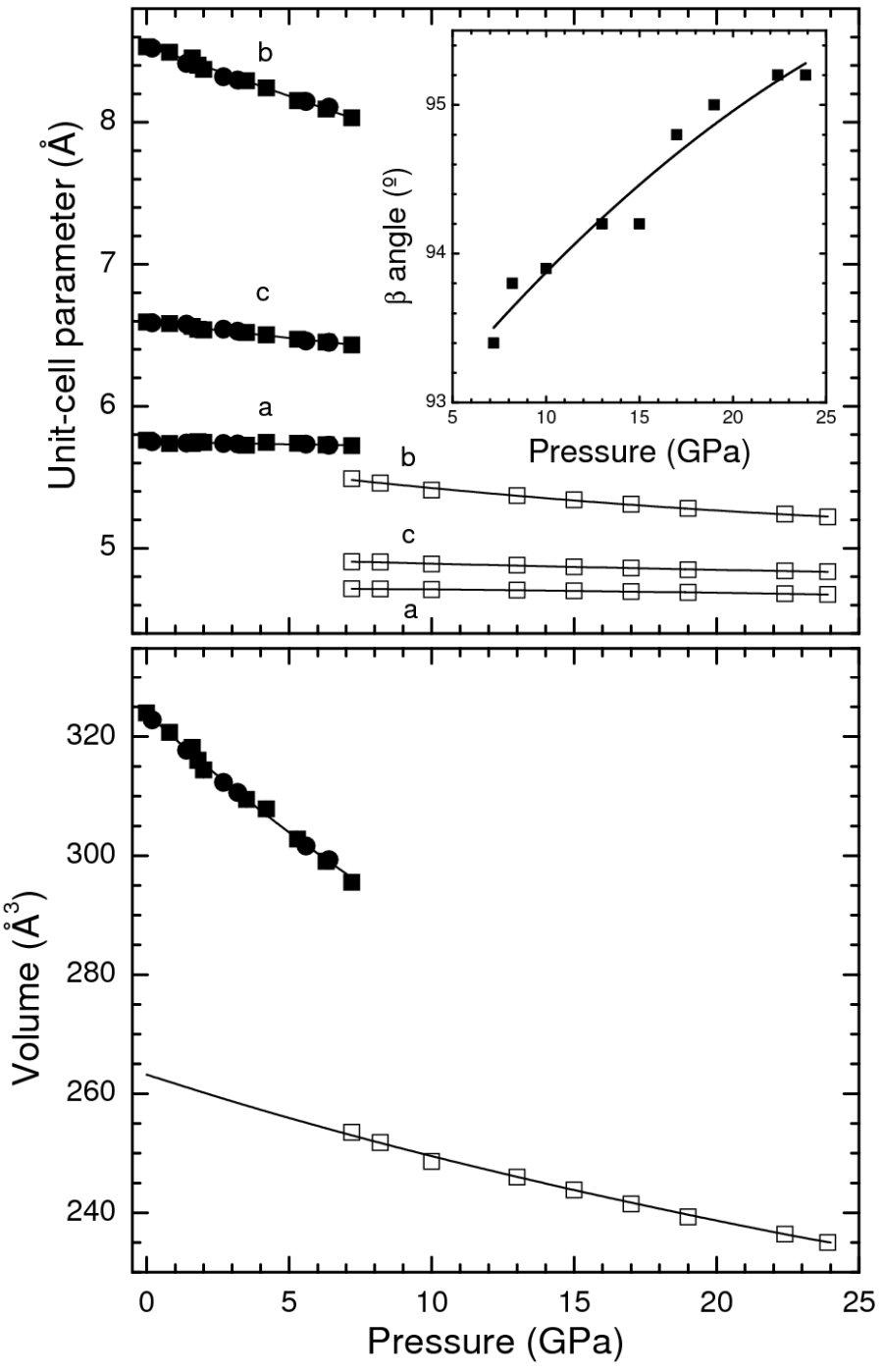

570 **Figure 4**

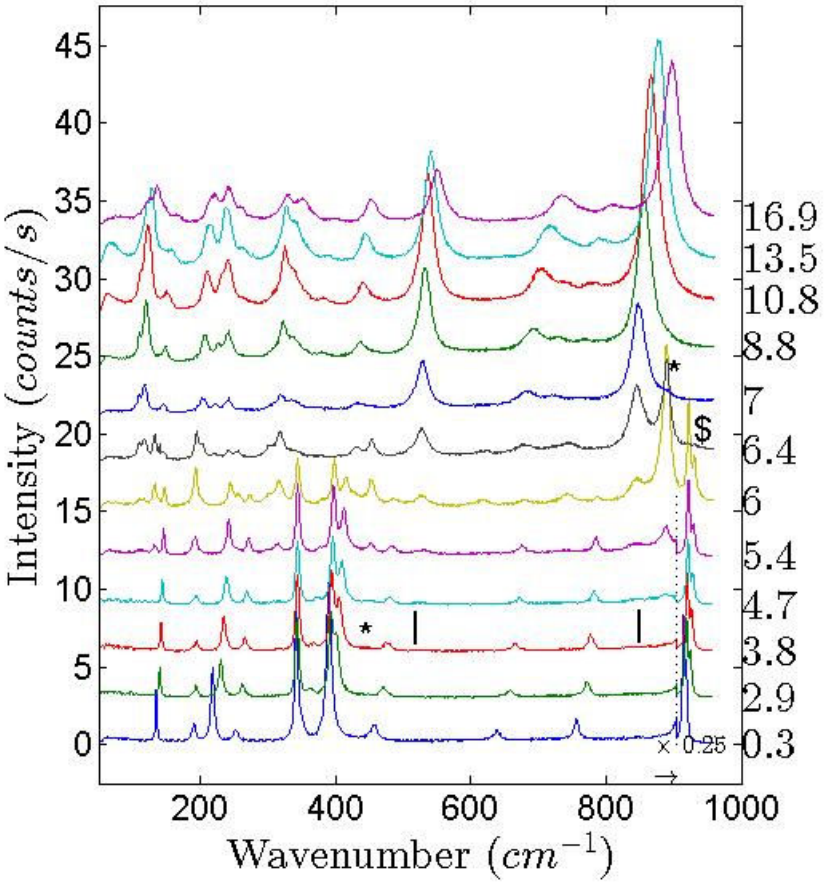
Intensity (counts/s)
Wavenumber (cm^{-1})
45
40
35
30
25
20
15
10
5
0
200
400
600
800
1000
16.9
13.5
10.8
8.8
7
6.4
6
5.4
4.7
3.8
2.9
0.3
*
$
x 0.25

Figure 5

598

599

600

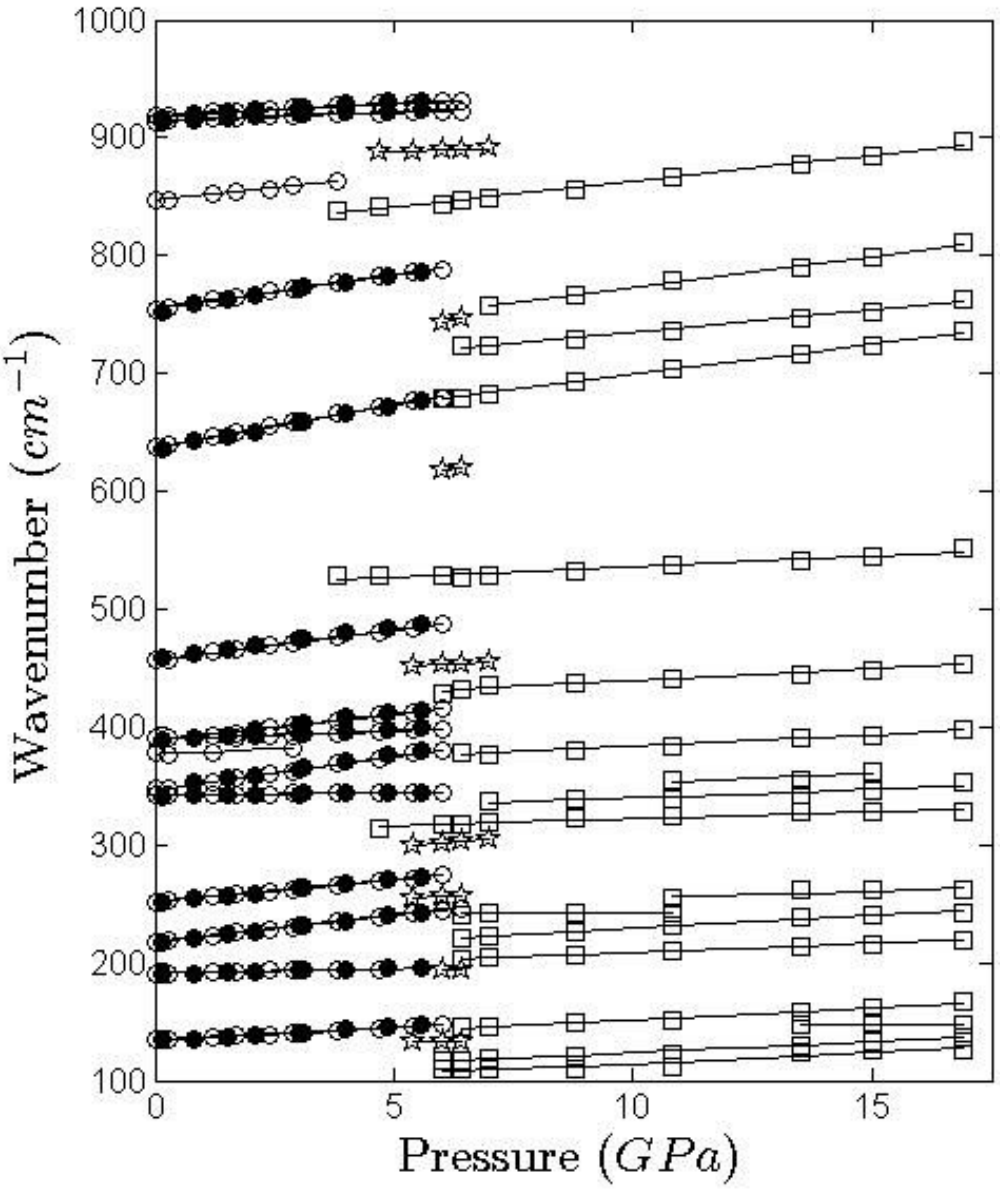

601

602 **Figure 6**

603

604

Table 1

$InVO_4$-III		$InVO_4$-V	
Pressure	0.8 GPa		8.2 GPa
Space group	*Cmcm*		*P2/c*
a	5.738(5) Å	*a*	4.714(5) Å
b	8.492(8) Å	*b*	5.459(6) Å
c	6.582(6) Å	*c*	4.903(5) Å
		β	93.8(3)º
V	320.72(2) $Å^3$		125.89(2) $Å^3$
Z = 4		Z = 2	
In (4a)	(0,0,0)	In (2f)	(0.5,0.711(1),0.25)
V (4c)	(0, 0.3617(5), 0.25)	V (2e)	(0, 0.159(1), 0.25)
O_1 (8g)	(0.2568(4), 0.4831(6), 0.25)	O_1(4g)	(0.214(2), 0.861(4), 0.492(2))
O_2 (8f)	(0, 0.7492(8), 0.9573(9))	O_2(4g)	(0.242(2), 0.407(3), 0.399(3))
B = 0.5 $Å^2$		B = 0.5 $Å^2$	
R_p	4.96 %		6.32 %
R_{wp}	7.40%		8.79%
In-O_2 (x2)	2.1483(6) Å	In-O_1 (x2)	2.0268(6) Å
In-O_1 (x4)	2.1623(6) Å	In-O_2 (x2)	2.1397(6) Å
		In-O_2 (x2)	2.2101(6) Å
V-O_2 (x2)	1.6579(5) Å	V-O_1 (x2)	1.6730(5) Å
V-O_1 (x2)	1.7983(5) Å	V-O_1 (x2)	2.2166(6) Å
		V-O_2 (x2)	1.8861(5) Å

611 **Table 2**

Orthorhombic Phase III			
	ω_0 [45]	ω_0	$\left(d\omega/dP\right)_0$
ω_1		135	2.1
ω_2		191	0.7
ω_3		218	4.5
ω_4		252	3.6
ω_5	342 (ν_2)	342	0.4
ω_6		348	5.6
ω_7		377	1.9
ω_8		389	4.4
ω_9	404 (ν_4)	390	1.4
ω_{10}	456	456	5.2
ω_{11}	640	637	7.2
ω_{12}	755 (ν_3)	755	5.7
ω_{13}		847	4.2
ω_{14}		914	1.3
ω_{15}	915 (ν_1)	918	2.1

612

613

614 **Table 3**

Phase V		
	ω (7 GPa)	$\left(d\omega/dP\right)$
ω_1	109	1.8
ω_2	118	1.9
ω_3	145	2.0
ω_4	149	-0.1
ω_5	204	1.5
ω_6	223	2.2
ω_7	241	0.0
ω_8	251	1.1
ω_9	319	1.2
ω_{10}	336	1.4
ω_{11}	347	1.6
ω_{12}	378	1.9
ω_{13}	433	2.0
ω_{14}	531	1.8
ω_{15}	684	5.1
ω_{16}	723	3.8
ω_{17}	758	5.2
ω_{18}	850	4.4

Phase IV		
	ω (7 GPa)	$\left(d\omega/dP\right)$
ω_1	133	0.1
ω_2	197	4.0
ω_3	258	1.8
ω_4	305	3.0
ω_5	455	1.7
ω_6	622	5.0
ω_7	750	6.7
ω_8	891	1.1

615

616

Table of contents synopsis

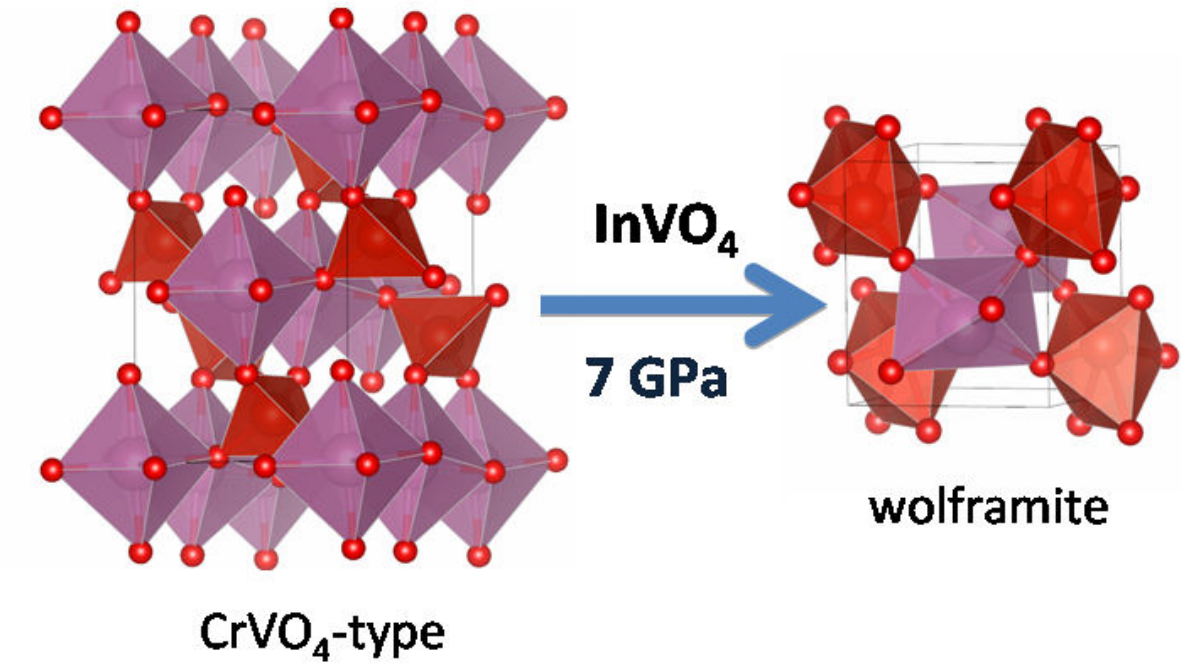

Two HP phases are detected in $InVO_4$ by XRD and Raman spectroscopy. For one of them, found beyond 7 GPa, a wolframite-type structure is assigned. This HP phase implies a coordination change for V, whose coordination number is increased from 4 to 6. The phase transition involves changes in the electronic structure of $InVO_4$ causing a band-gap collapse. The crystal structure of the different phases and the RT P-V equations of state are determined. Raman-active phonons are characterized for the different phases and their pressure behaviour determined.